

Prediction and Validation of the Process Window for Atomic Layer Etching: HF Exposure on TiO_2

Published as part of *The Journal of Physical Chemistry* virtual special issue "Dor Ben-Amotz Festschrift".

Suresh Kondati Natarajan,* Austin M. Cano, Jonathan L. Partridge, Steven M. George, and Simon D. Elliott



Cite This: *J. Phys. Chem. C* 2021, 125, 25589–25599



Read Online

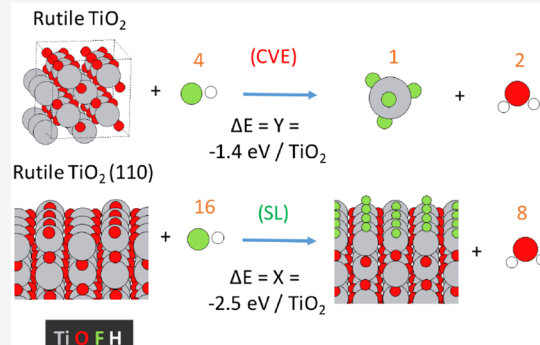
ACCESS |

Metrics & More

Article Recommendations

Supporting Information

ABSTRACT: A combined computational and experimental study is employed to understand the competition between self-limiting (SL) and chemical vapor etch (CVE) reactions to design an atomic layer etch (ALE) process. The pulses in an ALE process have to be self-limiting; i.e., the reactions should reach saturation after sufficient pulse time. By comparing the reaction free energies of corresponding SL and CVE reactions using density functional theory (DFT), the temperature and pressure conditions can be predicted that favor the SL or CVE reactions. The etching of TiO_2 when exposed to HF gas is utilized as a test case. Simulations reveal that when TiO_2 is exposed to reactant HF at a pressure of 0.2 Torr, the SL reaction removing H_2O at 0.01 Torr and fluorinating the surface is preferred up to 87 °C (360 K). At higher temperatures, continuous removal of TiO_2 by CVE occurs according to the reaction $\text{TiO}_2 + \text{HF} \rightarrow \text{TiF}_4 + \text{H}_2\text{O}$ subject to kinetic activation barriers. Experimental results from *in situ* Fourier transform infrared (FTIR) spectroscopy and quadrupole mass spectrometry (QMS) are compared with the theoretical predictions. In good agreement with theory, the FTIR spectroscopy studies revealed an onset of spontaneous etching (CVE) at temperatures around 80–90 °C. In addition, the QMS analysis observed TiF_4 and H_2O as the etch products, further validating the calculations. The calculations also predicted that an increase in the reactant gas pressure would enhance etching at high temperatures. The low computational cost of this theoretical approach allows for rapid screening of etch reagents and prediction of the temperature/pressure windows where the reactions will be in the SL or CVE regimes.



I. INTRODUCTION

Materials may be processed reliably and uniformly with atomic level control by exploiting self-limiting gas–surface reactions. For instance, atomic layer deposition (ALD) is a process in which a precise fraction of a monolayer of material is deposited in each cycle of gas pulses via a sequence of self-limiting (SL) surface reactions.^{1,2} ALD has become an indispensable step in the fabrication of modern semiconductor devices.^{1–5} Alternatively, materials may be deposited faster, but with less control, by means of chemical vapor deposition (CVD), which is a spontaneous and continuous process.

A sequence of SL reactions is also the basis for the atomic layer etch (ALE) process.^{6,7} ALE is expanding in scope to become a key enabling technology for the fabrication of next generation semiconductor devices. In some cases, combining ALD and ALE will be advantageous for the production of ultrasmooth thin films only on selected substrates.⁸ This area-selectivity could reduce the number of lithographic steps and allow further size reduction in semiconductor devices.^{6,8} The challenge is to identify SL chemistries, or more precisely, to

identify reagents and reaction conditions for the desired SL reaction. This paper presents a combined experimental and computational approach for meeting this challenge.

In the ALE concept, the target material surface is first chemically modified by exposure to a pulse of a suitable gas reactant that self-limits after forming a nonvolatile surface layer.^{7,9,10} The modified layer is then volatilized by the action of the second reactant pulse. Plasma ALE employs directional (i.e., anisotropic) high energy ion bombardment in the second pulse to remove the modified surface layer.^{7,11} Thermal isotropic ALE processes have also recently been introduced where the modified layer is removed by chemical reaction with another gas phase reactant.^{9,10,12} The second reactant may

Received: September 14, 2021

Revised: October 24, 2021

Published: November 12, 2021



ACS Publications

© 2021 American Chemical Society

25589

<https://doi.org/10.1021/acs.jpcc.1c08110>
J. Phys. Chem. C 2021, 125, 25589–25599

then remove the entire modified layer in a continuous, unlimited way, but it self-limits upon reaching the unmodified material underneath.

Modification of the surface by the first reactant is the subject of this study. The first reactant is introduced into the etch chamber as a gas and adsorbs onto the substrate material by binding with the surface atoms. A volatile byproduct may be produced at this stage. If some fragment of the reactant passivates the surface and causes the surface to become inert toward further reactant adsorption, then this is an SL reaction, as required for ALE.¹³ On the other hand, the adsorbate could continue to react with the substrate by diffusing into and reacting with subsurface layers. This process would result in continual formation of volatile byproducts that desorb and regenerate active sites on the surface. This spontaneous reaction would be a CVE process.¹³

Thermochemical calculations of model reactions have been performed by researchers investigating ALD and ALE processes.^{10,14–20} One popular approach is to model the reactions using thermochemical tables from databases such as NIST-JANAF²⁰ with the help of software packages such as the HSC Chemistry.²¹ Alternatively, reactions can be modeled from first-principles using density functional theory (DFT) calculations. Such calculations have been used to investigate ALD mechanism in detail^{13,14,22} and recently also to study thermal ALE with HF.^{13,23} One advantage of using first-principles calculations is that any specific phase of a solid system or any gas phase molecule of interest, however exotic, can be modeled explicitly by ab initio methods. In addition, databases typically include only bulk materials, and so the calculated thermochemistry is valid only for bulk deposition or etching, and not for the surface reactions.

Applying DFT to a slab model is the standard computational procedure for investigating material surfaces, including their interaction with gas phase molecules.^{13,23} This approach can be used to model the SL reaction. By comparing the free energy profiles (FEPs) of CVE and SL reactions using the “Natarajan–Elliott” analysis,¹³ the nature of a reactant pulse can be understood. From this analysis, a “minimum thermodynamic barrier” to etch is computed, which is the difference between the corresponding reaction free energies of the CVE and SL reactions. Four distinct reaction states are identified based on the value of this “minimum thermodynamic barrier”. These states are purely self-limiting, preferred self-limiting, preferred etching, and purely etching. A detailed description of this analysis methodology is given elsewhere.¹³

TiO₂²⁴ has significant applications in a variety of technological fields.²⁴ For example, TiO₂ is an important photocatalyst and has been explored for the production of hydrogen and self-cleaning surfaces.²⁵ TiO₂ is also a key material in semiconductor devices such as metal-oxide resistive random access memory (RRAM).²⁶ Thin films of TiO₂ are also used in mirror coatings, orthopedic implants and pharmacological applications. A great number of examples are available where thin films of TiO₂ have been deposited using the ALD approach.^{27,28}

HF has been used as the fluorinating agent in the thermal ALE of several metal oxides such as Al₂O₃, HfO₂ and ZrO₂.^{10,15,16} However, HF was found to be unsuitable in the thermal ALE of TiO₂ where the Ti atoms are in an oxidation state of +4.²⁹ TiO₂ is spontaneously etched by HF at temperatures greater than 200 °C, probably forming gaseous TiF₄ and H₂O.²⁹ However, when WF₆ was used as the

fluorination reactant at lower temperatures below 170 °C, TiO₂ ALE was possible using WF₆ and BCl₃ without the spontaneous etching of TiO₂.¹⁷ Therefore, HF exposure on TiO₂ presents an excellent test case for investigating the competition between self-limiting and spontaneous etch reactions.

The purpose of this paper is to demonstrate and validate a combined computational and experimental approach for the design of new ALE processes. The main design steps are (1) choosing reactant molecules for each pulse, (2) optimizing the process conditions in terms of temperature and reactant gas pressure, and (3) identifying and treating the exhaust gases. In a purely experimental approach, each design choice is evaluated by trial and error in the laboratory. This is a time intensive process that limits the number of options that can be considered. On the other hand, a purely computer-based design can consider a much larger range of molecules. However, the computational model may not be able to include all the variables. A closely coupled combination of computations to narrow down the design choices and experiments to optimize the reaction conditions may provide the best strategy.

II. METHODS SECTION

II.A. Computational Methods. The calculations described in this paper were performed within spin-polarized density functional theory (DFT) using the Vienna ab initio simulation package (VASP, version 5.3).³⁰ The calculations were based on the generalized gradient approximation (GGA) using the Perdew–Burke–Ernzerhof (PBE) exchange-correlation functional.³¹ The core electrons were described by projector augmented wave potentials^{32,33} and the valence electrons were treated explicitly using plane wave basis sets up to 400 eV of energy.

The reaction free energies reported in this paper were computed as follows

$$\Delta G = G_p - G_r + RT \ln(Q)$$

with

$$G_{\text{plr}} = H_{\text{plr}} - TS_{\text{plr}}$$

$$H_{\text{plr}} = E_{\text{plr}} + \text{ZPE}_{\text{plr}} + W(T)_{\text{plr}}$$

$$Q = \prod p_{\text{p}}^{\mu} / \prod p_{\text{r}}^{\mu}$$

Here, ΔG is the reaction free energy, p and r in the subscript refer to products and reactants, respectively, H is the enthalpy, which includes the DFT electronic energy E and the zero point energy (ZPE), and S is entropy. The temperature-dependent enthalpy $W(T)$ is simply RT for molecules and $\sum_q \hbar\omega(q)/(\exp(\hbar\omega(q)/k_B T) - 1)$ for solids where q is wave vector, ν is phonon mode index, and ω is the phonon frequency. Q is the reaction quotient, which measures the relative amounts of product and reactant molecules participating in the reaction, and μ is the stoichiometric coefficient for the reaction. The quantities H and S for bulk and surface models were obtained from phonon frequencies using the Phonopy code.³⁴ Accurate force constants are a prerequisite for this, and they were obtained from density functional perturbation theory (DFPT) calculations in VASP using a strict energy convergence threshold of 1.0e⁻⁸eV.

“Natarajan–Elliott” analysis was used to study the competition between CVE and SL reactions via free energies from a modest number of DFT calculations. In this analysis, each precursor pulse is designated to one of four possible cases depending on the reaction free energies of the SL and CVE reactions (negative free energy means the reaction is favorable):¹³

- (a) preferred self-limiting ($\Delta G_{\text{CVE}} < 0$; $\Delta G_{\text{SL}} < \Delta G_{\text{CVE}}$),
- (b) purely self-limiting ($\Delta G_{\text{CVE}} > 0$; $\Delta G_{\text{SL}} < 0$; $\Delta G_{\text{SL}} < \Delta G_{\text{CVE}}$),
- (c) preferred etching ($\Delta G_{\text{CVE}}, \Delta G_{\text{SL}} < 0$; $\Delta G_{\text{SL}} > \Delta G_{\text{CVE}}$), and
- (d) purely etching ($\Delta G_{\text{CVE}} < 0$; $\Delta G_{\text{SL}} > 0$; $\Delta G_{\text{SL}} > \Delta G_{\text{CVE}}$).

The bulk and surface models of TiO_2 in the calculations were constructed from its rutile crystalline phase (space group $P42/mnm$), and the corresponding relaxed geometries are shown in Figure 1. The bulk unit cell consists of two TiO_2

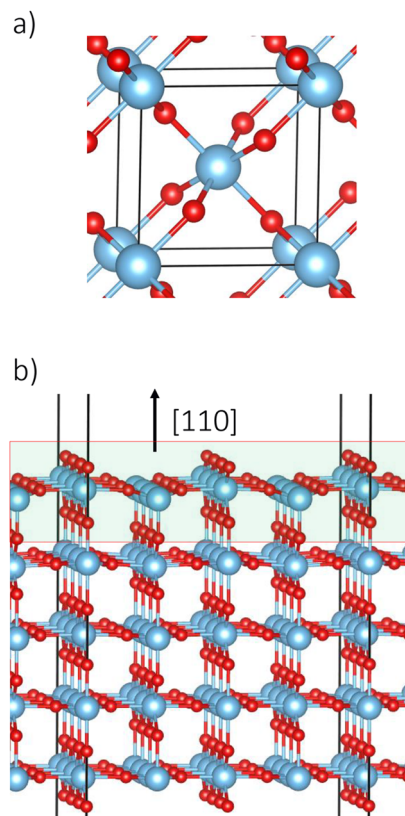


Figure 1. (a) Equilibrium bulk geometry of rutile TiO_2 . (b) Relaxed surface slab of $\text{TiO}_2(110)$. Ti and O atoms are displayed in cyan and red, respectively.

units, which are optimized by simultaneously relaxing the ionic positions, cell volume and cell shape with a higher energy cutoff of 550 eV and a Monkhorst–Pack k -point mesh of $6 \times 6 \times 6$. For the surface calculations, a 15 Å thick slab of (2×4) supercell of the rutile- TiO_2 (110) surface ($\text{Ti}_{80}\text{O}_{160}$) with a surface area of 1.57 nm^2 and relaxed surface energy of 0.91 J/m^2 was constructed with 15 Å of vacuum separating the periodic images in the surface normal direction. This supercell consists of 5 $\text{Ti}_{16}\text{O}_{32}$ layers, out of which the bottom two layers were kept fixed. A k -point mesh of $2 \times 2 \times 1$ was used for

geometry optimization of this slab. The (110) surface of rutile TiO_2 was chosen for this study as its signature was found from the XRD spectra of TiO_2 ALD at high film thicknesses.³⁵

To model the surface geometries resulting from the SL reactions, preserving stoichiometry, 8 surface O atoms are removed from the bare surface of $\text{TiO}_2(110)$ followed by the adsorption of 16 F atoms as shown in Figure 2a. Moreover, to

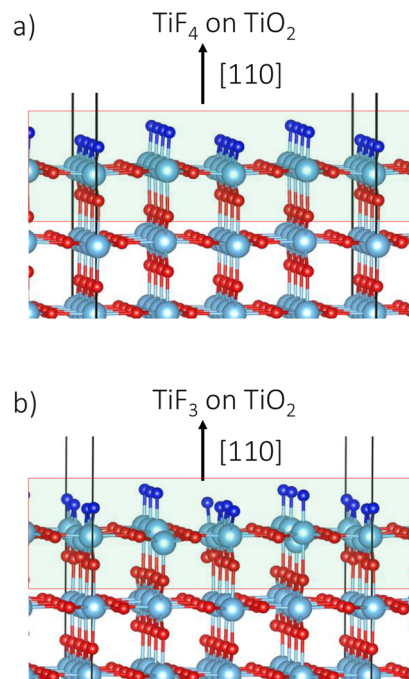


Figure 2. (a) Relaxed surface slab model of self-limited fluorination of $\text{TiO}_2(110)$ as “ TiF_4 ”. (b) Relaxed surface slab model of self-limited fluorination of $\text{TiO}_2(110)$ as “ TiF_3 ”.

represent the reduced TiO_{2-x} surface, just 12 F atoms are adsorbed following the removal of 8 O atoms as shown in Figure 2b. For these surface slabs, H and S are computed by considering only the top layer of surface atoms highlighted in the figures.

Gas phase calculations of the reagent molecules and byproducts were performed using VASP with a large periodic box of dimensions $15.0 \text{ \AA} \times 16.0 \text{ \AA} \times 15.5 \text{ \AA}$ with an energy cutoff of 400 eV. However, for convenience, H and S values for these gas phase molecules are obtained from the “freeh” program of the Turbomole suite³⁶ at a constant pressure of 1 atm. All gas phase calculations in Turbomole were performed with the PBE functional and a valence triple- ζ basis set (def-TZVPP).

II.B. Experimental Methods. For the FTIR studies of etching, TiO_2 ALD films were first deposited on silicon nanopowder covered with native oxide (>98% US Research Nanomaterials) that had an approximate diameter of 30 nm. This nanopowder was used to achieve a high TiO_2 surface area for greater signal-to-noise for the FTIR experiments.³⁷ The powder was pressed into a $1.5 \text{ cm} \times 3 \text{ cm}$ tungsten grid that was $50 \mu\text{m}$ thick with 100 grid lines per inch.³⁷ The tungsten grid was resistively heated with a DC power supply (6268B, 12 V/40 A, HP) to heat to the temperatures needed for the ALD and spontaneous etching experiments. The power supply was controlled by a PID temperature controller (Love Controls

Table 1. Reaction Energies (ΔE) of the Postulated CVE (Y) and SL (X) Reactions Representing the HF Pulse on TiO_2 along with the Corresponding ‘Minimum Thermodynamic Barrier’ (Y-X) to Etch^a

	reactions	ΔE [eV/u.b.]	Y-X [eV/u.b.]
CVE1	$\text{TiO}_{2(b)} + 4\text{HF}_{(g)}\text{TiF}_{4(g)} + 2\text{H}_2\text{O}_{(g)}$	Y1 = -1.4	1.1
SL1	$\text{TiO}_{2(surf)} + 4\text{HF}_{(g)}\text{TiF}_{4(surf)} + 2\text{H}_2\text{O}_{(g)}$	X1 = -2.5	
CVE2	$\text{TiO}_{2(b)} + 2\text{HF}_{(g)}\text{TiOF}_{2(g)} + 1\text{H}_2\text{O}_{(g)}$	Y2 = 2.0	3.3
SL2	$\text{TiO}_{2(surf)} + 2\text{HF}_{(g)}\text{TiOF}_{2(surf)} + 1\text{H}_2\text{O}_{(g)}$	X2 = -1.3	
CVE3	$\text{TiO}_{2(b)} + 3\text{HF}_{(g)}\text{TiF}_{3(g)} + 1.5\text{H}_2\text{O}_{(g)} + 0.25\text{O}_{2(g)}$	Y3 = 2.1	2.5
SL3	$\text{TiO}_{2(surf)} + 3\text{HF}_{(g)}\text{TiF}_{3(surf)} + 1.5\text{H}_2\text{O}_{(g)} + 0.25\text{O}_{2(g)}$	X3 = -0.4	

^aThe energy values are normalized per unit bulk (u.b.) material. (b) refers to bulk, (g) to gas-phase and (surf) to surface.

16B, Dwyer Instruments). To monitor the temperature, a type K thermocouple was connected to the tungsten grid with a non conductive epoxy (Cermabond 571).

TiO_2 ALD was performed in a home-built warm-walled ALD reactor equipped for FTIR studies as described previously.^{38,39} For sample temperatures greater than 150 °C, the chamber walls were held at 150 °C and the sample was heated using the DC power supply. For sample temperatures below 150 °C, the temperature of the chamber walls controlled the sample temperature. TiO_2 ALD was accomplished with sequential exposures of TiCl_4 ($\geq 99.995\%$ trace metals basis, Sigma-Aldrich) and H_2O at 200 °C.^{27,28,39,40} The TiCl_4 and H_2O reactants produce a TiO_2 ALD growth rate of $\approx 0.4 \text{ \AA/cycle}$ at 200 °C.^{28,40} The resulting TiO_2 ALD films are amorphous by X-ray diffraction analysis and known to have low chlorine concentrations of ≈ 1 at% by X-ray photoelectron spectroscopy measurements.^{28,40}

During the TiO_2 ALD process, the TiCl_4 half-cycle was a 2 s exposure at 50–100 mTorr in viscous flow with the N_2 carrier gas. The TiCl_4 exposure was followed by purging with the N_2 carrier gas for 90 s. Then the FTIR spectrum was acquired during a scan for 60 s. The H_2O half-cycle consisted of a 1 s exposure at 50–80 mTorr in viscous flow with the N_2 carrier gas. The H_2O exposure was followed by purging with the N_2 carrier gas for 60 s. Then the FTIR spectrum was acquired during a scan for 60 s.

For HF exposures on TiO_2 , each HF exposure was a 2 s exposure at 200 mTorr in viscous flow with the N_2 carrier gas. The HF exposure was followed by purging with the N_2 carrier gas for 90 s. Then the FTIR spectrum was acquired during a scan for 60 s. Longer purges than necessary for ALD were used to reduce the possibility of HF contact with the KBr windows during the FTIR scan. Spectra were recorded with a spectral resolution of 4 cm^{-1} . Prior to the etching experiments at different temperatures, the sample was equilibrated at each temperature for 30 min.

The QMS investigations employed a new reactor that has been described earlier.⁴¹ This reactor allows the study of etch products produced by flowing reactant gases through powder samples. The etch products and background gas are then expanded through an aperture and form a molecular beam. The beam of background gas and etch products are then passed through a skimmer and enter a differentially pumped region for QMS analysis. The details of this apparatus have been given previously.⁴¹

The skimmer aperture diameter was 1.4 mm, and the skimmer was positioned 41 mm from the sample aperture. The volatile etch products were observed using a high sensitivity, high mass quadrupole mass spectrometer (Extrel, MAX-QMS Flanged Mounted System). Each spectrum was recorded in 1 s and monitored mass intensities from 1 to 500 amu. After the

position of the products was determined, the mass spectrum was recorded from 30 to 300 amu using optimized ionization energy and electron multiplier gain. An average of 100 scans were recorded during HF exposures to eliminate noise. Electron-impact ionization of gas-phase etching products was achieved with a circular thoriated iridium filament in the ionization volume inside the ionizer housing. An electron ionization energy of 70 eV was used for these experiments.

HF was first introduced into a reservoir at a pressure of 9 Torr to have a consistent HF partial pressure during the reaction. HF was leaked into the flowing N_2 background gas. The HF pressure in the sample holder containing the TiO_2 powder was 5.2 Torr. The background N_2 pressure was 2.8 Torr. TiO_2 nanopowder was purchased from US Research Nanomaterials (99.9%, 165 nm diameter) and added to a sample holder. The mass of the TiO_2 nanopowder was recorded before and after the etching experiments. The mass of the nano powder before etching was 40.58 mg.

III. RESULTS

III.A. Computational Results. **III.A.1. Computed Energies of HF Reactions with TiO_2 .** The possible CVE and SL reactions representing the HF pulse on TiO_2 are listed in Table 1 along with their corresponding reaction energies computed with DFT. Three sets of CVE and SL reactions are postulated for the TiO_2 and HF interaction. In the CVE1 reaction of TiO_2 , four HF molecules are needed to etch away one unit of bulk as TiF_4 and H_2O , whereas in the CVE2 reaction, two HF molecules are assumed to be enough to etch a unit of TiO_2 by forming TiOF_2 and H_2O . These two reactions are of nonredox type since the Ti ion in the product species retains the oxidation state of +4. On the other hand, in the CVE3 reaction, the Ti^{4+} ion in TiO_2 is reduced to Ti^{3+} by forming TiF_3 . The CVE2 and CVE3 reactions are computed to be unfavorable at 0 K with positive reaction energies while the CVE1 reaction is exoergic.

Surface-limited versions of these three reactions are also postulated. The SL1, SL2, and SL3 reactions of TiO_2 are found to be energetically more favorable than the CVE1, CVE2, and CVE3 reactions, respectively. This behavior can be interpreted as the TiF units bonded on the surface being much more favorable than TiF_x molecules in the gas phase at 0 K. CVE1 and SL1 are the most favorable reactions for TiO_2 since the minimum thermodynamic barriers (differences between CVE and SL reaction energies) of the other reaction sets are significantly larger. Therefore, the energy profile of the HF pulse at $T = 0$ K falls under the “preferred self-limiting” category as both SL and CVE are energetically allowed, but with CVE facing a minimum thermodynamic barrier of 1.1 eV/ TiO_2 .

III.A.2. Reaction Free Energy Profiles for Etching of TiO_2 . FEPs of the candidate etching reactions in Table 1 are computed with a reactant pressure of 0.2 Torr and product pressure of 0.01 Torr in the temperature range 0 to 1000 K. The various contributions to the free energy of the CVE1 reaction of TiO_2 are plotted in Figure 3. ΔE and ΔZPE do not

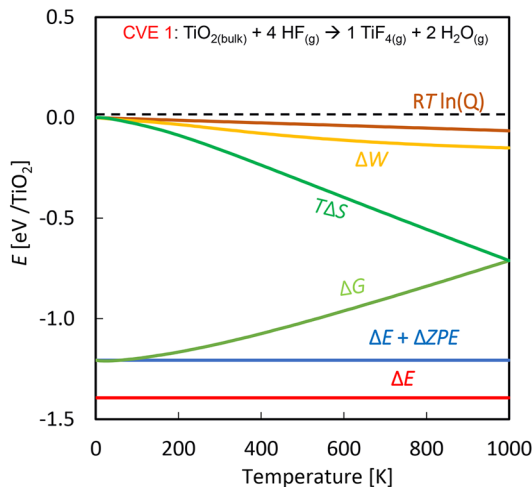


Figure 3. Various contributions to the reaction FEP for the CVE1 reaction of $\text{TiO}_2 + \text{HF} \rightarrow \text{TiF}_4 + \text{H}_2\text{O}$ at an HF reactant pressure of 0.2 Torr.

change with temperature and are represented as horizontal lines. The entropy term, $T\Delta S$, dominates the FEP of this reaction by spanning from 0 eV at 0 K to -0.73 eV per bulk unit at 1000 K. The entropy decreases primarily because four gaseous molecules react to produce only three product molecules, which indicates that the relative entropies of reactant and product gases play a crucial role in the temperature-dependence of the etch process. The $RT \ln(Q)$ and ΔW terms contribute relatively little in magnitude compared with the entropy term at this pressure. However, these terms do have the effect of offsetting some of the entropic increase in free energy at high temperature for CVE1. At these reactant and product pressures, the FEP shows that the CVE1 reaction is exergonic ($\Delta G < 0$) up to at least 1000 K.

The FEPs of CVE and SL reactions for TiO_2 can be compared as shown in Figure 4. The CVE2 and CVE3 reactions have almost identical FEPs and are endergonic even though their FEPs have a negative slope. In contrast, the CVE1 reaction is fully exergonic even though its FEP has a slightly positive slope. At some very high temperature, the ΔG profiles of CVE1 and CVE2 may cross over each other. In that case, CVE2 producing TiOF_2 would become the most favorable etch reaction. However, judging from the slopes of their FEPs, CVE2 and CVE3 will not cross each other. Consequently, the formation of volatile TiF_3 will never be more favorable than the formation of volatile TiOF_2 .

The SL reactions are comparatively more exoergic than the CVE counterparts at low temperatures up to 360 K (87°C). The HF molecules passivate the TiO_2 surface and form surface-bound products in the SL reactions. As a result, there is a significant entropic penalty that is evident in the strongly positive slope of the FEPs of the SL reactions. The SL3 reaction is unfavorable at all temperatures above 70 K, which

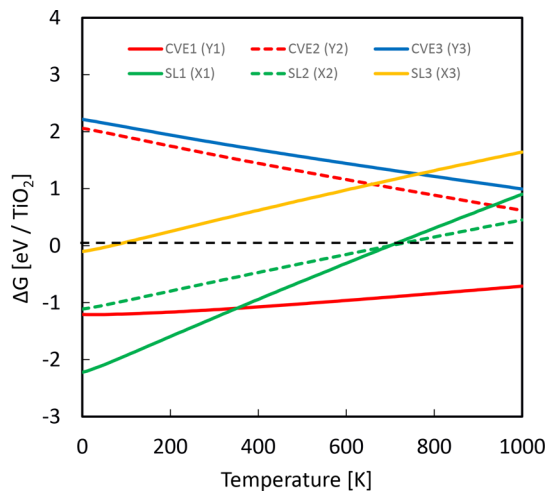


Figure 4. FEPs for the CVE1, CVE2, CVE3, SL1, SL2, and SL3 reactions for HF interacting with TiO_2 versus temperature. The labels X and Y correspond to the values listed in Table 1.

indicates that reduction by HF of surface Ti atoms to TiO_{2-x} is unlikely.

Considering only the most favorable reactions, CVE1 and SL1, the graph in Figure 5 can be divided into three regions.

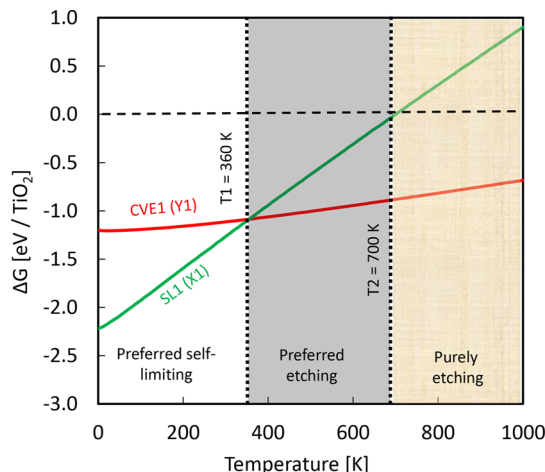


Figure 5. FEPs of CVE1 and SL1 showing three regions: preferred self-limiting, preferred etching, and purely etching. SL1 and CVE1 line crossing occurs at 360 K (87°C).

The FEPs of the CVE1 and SL1 reactions cross at 360 K (87°C). The region between 0 and 360 K is labeled as “preferred self-limiting”, since the SL1 reaction is the most favorable in this region and the ‘minimum thermodynamic barrier’ for SL1 to CVE1 is positive. HF etching of the bulk by CVE1 is possible in this region if the energetic barrier, including kinetic requirement, can be overcome at the reactor conditions. The “minimum thermodynamic barrier” drops from a value of 1.1 eV per bulk unit at 0 K to zero at 360 K where the CVE1 and SL1 reactions become equally favorable for producing byproducts at pressure of 0.01 Torr.

The region between 360 K (87°C) and 700 K (427°C) is called “preferred etching”, since fluorination of the surface by reaction SL1 is possible, but the CVE1 reaction to volatile TiF_4 is more favored. The actual etch pathway may face kinetic barriers that have not been computed in this study. While

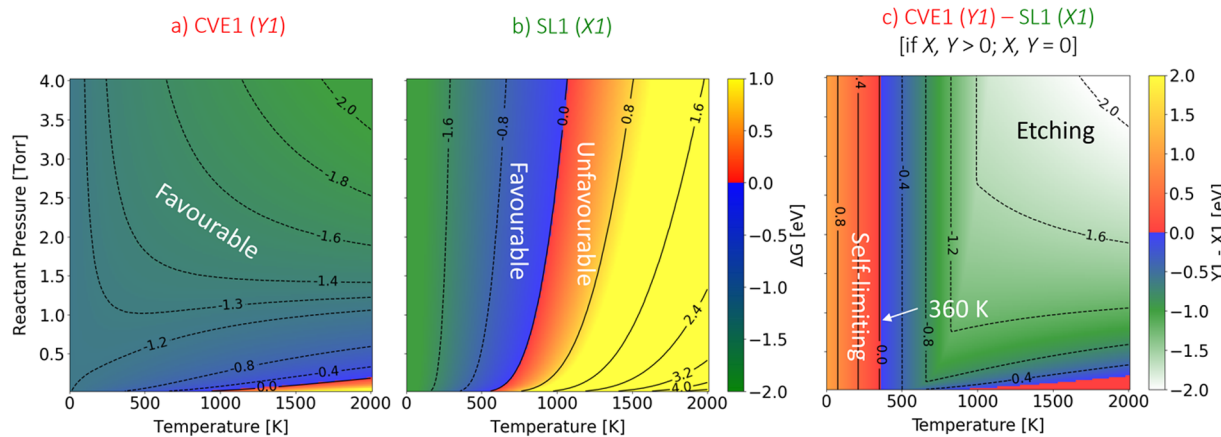


Figure 6. “Heat” maps showing the change in free energy of (a) CVE1 and (b) SL1 reactions for HF exposure on TiO_2 . (c) Change in corresponding minimum thermodynamic barrier with respect to reactant pressure and temperature.

computing the entire mechanism and associated kinetics would always be the ideal approach, resource limitations may not allow it. The SL1 reaction becomes endergonic beyond 700 K, and this temperature region is labeled “purely etching”. This label suggests that, at these high temperatures, the surface may resist fluorination via SL1, which may constitute a barrier toward the formation of volatile TiF_4 (for CVE1), though we have no data on such details of the mechanism.

III.A.3. Influence of Reactant and Product Pressures. The etch reactions have been considered above at a constant reactant (HF) pressure of 0.2 Torr and a byproduct pressure of 0.01 Torr. The reactant gas pressure can be controlled in the reactor. However, the product pressure is not an experimentally adjustable parameter. Any change in the reactant and product pressures will alter the slope of the FEPs due to the contributions from the $RT \ln(Q)$ term, and will hence change the process window. This is now shown for the CVE1 and SL1 reactions of TiO_2 under changes in reactant (HF) pressure from 0.01 to 4 Torr at a constant byproduct pressure of 0.01 Torr.

Parts a and b of Figure 6 display color maps showing the free energy changes of the CVE1 and SL1 reactions of TiO_2 along with the minimum thermodynamic barrier for etching (CVE1-SL1) in Figure 6c. The CVE1 reaction shown in Figure 6a is mostly favorable in the entire reactant pressure range. CVE1 also becomes more favorable at high temperatures and high reactant pressure. Consequently, an increase of the reactant pressure decreases the slope of the FEP of the CVE1 reaction. In the SL1 reaction shown in Figure 6b, the favorable region is pushed to higher temperatures at higher reactant pressure.

From the minimum thermodynamic barrier map in Figure 6c, the SL1 reaction is computed to be preferred up to 360 K (87 °C) for the entire reactant pressure range. This means that the temperature at which the FEPs of the CVE1 and SL1 reactions cross over is constant with respect to increase in the reactant pressure, under the assumption of a constant product pressure. This behavior occurs because the number of reactant HF molecules per unit TiO_2 is the same for both CVE1 and SL1 reactions. In the “purely etching” region ($\Delta G(\text{SL1}) > 0$ and $\Delta G(\text{CVE1}) < 0$), the minimum thermodynamic barrier to etch decreases at higher reactant pressure.

III.B. Experimental Results. III.B.1. FTIR Spectroscopy. Figure 7 shows the progressive growth of a TiO_2 film during 36 ALD cycles on silicon nanoparticles measured by the infrared

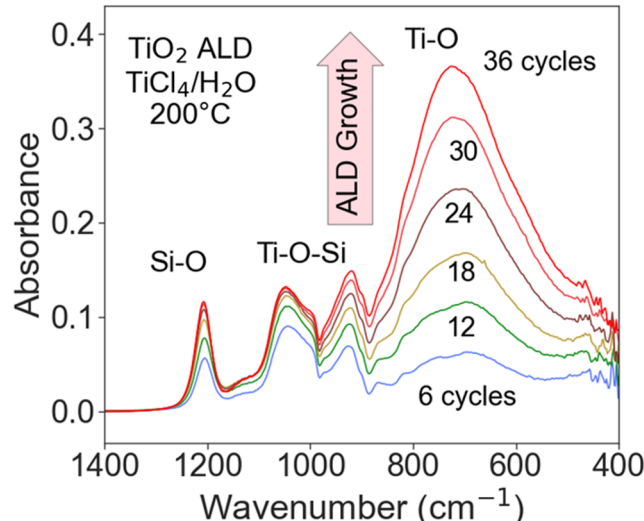


Figure 7. FTIR absorbance during TiO_2 ALD on silicon nanoparticles at 200 °C versus number of ALD cycles using TiCl_4 and H_2O as the reactants.

absorbance. TiCl_4 and H_2O were employed as the reactants at 200 °C for TiO_2 ALD. The spectra are referenced to the original silicon nanoparticle sample that has a thin native oxide of the silicon surface. The absorption peak at 400–960 cm^{-1} corresponds to Ti–O stretching vibrations.^{42,43} The Ti–O stretching vibrations yield a peak at 722 cm^{-1} that increases linearly with number of TiCl_4 and H_2O cycles.

The initial cycles of TiO_2 ALD also give rise to several other absorption peaks at 1209, 1048, and 940 cm^{-1} . The vibrational band at 1209 cm^{-1} is assigned to Si–O vibrations that arise due to the oxidation of the silicon powder with H_2O exposures.^{44,45} This peak grows rapidly during the first 10 TiO_2 ALD cycles, and then the growth slows at higher TiO_2 ALD film thicknesses. The bands at 940 and 1048 cm^{-1} are assigned to Si–O–Ti vibrations resulting from the mixing of TiO_2 and SiO_2 at the interface.^{46,47} These vibrational bands also do not increase further as TiO_2 ALD continues past 30 cycles.

The etching of the TiO_2 ALD films by HF was studied by monitoring the changes to the FTIR spectrum. Another TiO_2 ALD film was grown using multiple TiO_2 ALD cycles. Figure 8

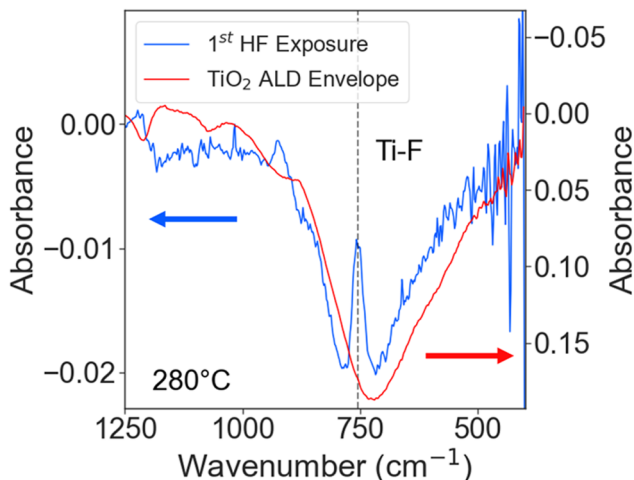


Figure 8. FTIR difference spectrum for the first HF exposure on TiO_2 . Difference spectrum was obtained using the FTIR absorbance spectrum for TiO_2 ALD after 36 cycles as a reference. Absorbance for the TiO_2 ALD film after 36 cycles is also shown for comparison

shows the difference spectrum after the first exposure of HF at 200 mTorr for 2 s at 280 °C. This difference spectrum is referenced to the infrared spectrum from the last 20 cycles used to grow the TiO_2 ALD film. The vertical axis for this reference spectrum has been scaled and shown in Figure 8. The comparison between the difference spectrum and the reference spectrum reveals that the HF exposure removes the TiO_2 ALD film. The difference spectrum displays a broad decrease in absorbance at 400–960 cm^{-1} that is consistent with the spectrum for the TiO_2 ALD film.

There is also a new feature in Figure 8 that is not in agreement with the loss of the absorbance from the $\text{Ti}-\text{O}$ stretching vibration. This feature is observed as an absorption peak at 777 cm^{-1} . This absorption feature is assigned to a $\text{Ti}-\text{F}$ stretching vibration.^{48,49} The difference spectrum is consistent with the HF exposure spontaneously etching TiO_2 and leaving the TiO_2 surface terminated with $\text{Ti}-\text{F}$ species after the HF exposure. This $\text{Ti}-\text{F}$ surface species may be viewed as an intermediate on the way to volatile etch species. The expected possible volatile etch products from the spontaneous etching of TiO_2 by HF may be TiF_4 or TiOF_2 , which is checked by QMS measurements and DFT calculations.

Figure 9 shows the difference spectra after 10 HF exposures at 200 mTorr for 2 s at 280 °C. The starting sample was a TiO_2 ALD film deposited after 60 ALD cycles. The difference spectra are referenced to the absorption spectrum for this TiO_2 ALD film. The decrease of the absorbance for the $\text{Ti}-\text{O}$ stretching vibration between 500 and 900 cm^{-1} in Figure 9 is linear with respect to the HF exposure. The continuous loss of TiO_2 indicates spontaneous etching (CVE) during each HF exposure.

Figure 9 also provides confirmation that the absorption feature at 777 cm^{-1} corresponds to a $\text{Ti}-\text{F}$ surface species. This absorption peak at 777 cm^{-1} persists through the first, third, fifth, and 10th HF exposures. The size of this absorption feature also remains constant during the ten HF exposures. These results are expected since the surface area of $\text{Ti}-\text{F}$ surface species stays constant as the TiO_2 ALD film is progressively removed by spontaneous etching.

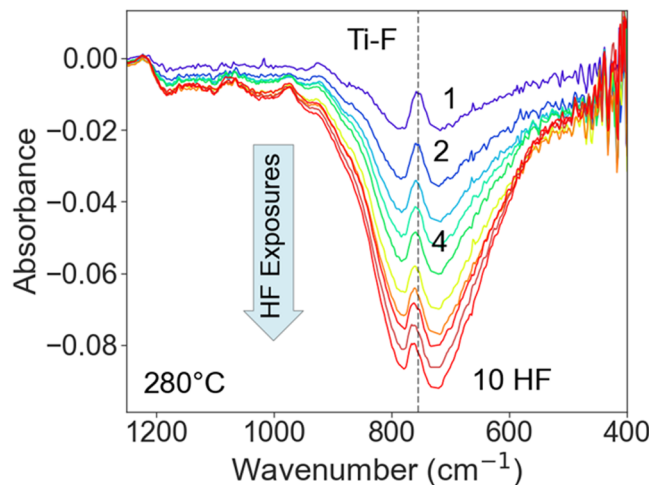


Figure 9. FTIR difference spectra after 10 sequential HF exposures at 280 °C on TiO_2 ALD films. Absorbance feature at 777 cm^{-1} is assigned to $\text{Ti}-\text{F}$ stretching vibration.

The spontaneous etching of TiO_2 increases at higher substrate temperature. To quantify the spontaneous etching rate, experiments were performed at 14 different temperatures between 80 and 300 °C. The change in FTIR absorbance was integrated over the frequency range 400 to 960 cm^{-1} after each HF exposure for 10 HF exposures at each temperature. This change in the integrated absorbance during each HF exposure is proportional to the TiO_2 etch rate, which is shown in Figure 10. There is a small but measurable integrated absorbance loss at temperatures as low as 80 °C (353 K), but not at lower temperatures. The TiO_2 etching starts to increase more noticeably at approximately 150 °C (423 K). The etch rate increases progressively with temperature up to 300 °C (573 K). These results for the spontaneous etching of TiO_2 are in agreement with previous experiments that revealed the

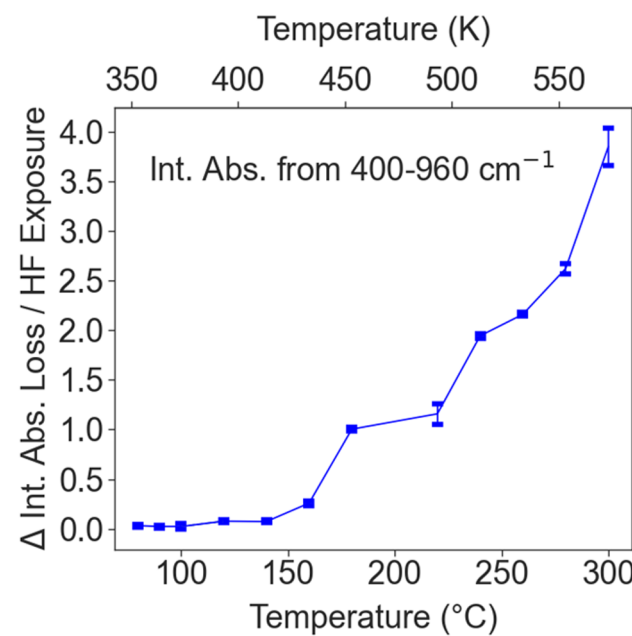


Figure 10. Etch rate as measured by change in integrated absorbance of the $\text{Ti}-\text{O}$ vibrational modes from 400 to 960 cm^{-2} for each HF exposure. Temperature is varied from 80 to 300 °C.

spontaneous etching of TiO_2 ALD films by HF exposures at 200, 250, and 300 °C using quartz crystal microbalance (QCM) measurements.²⁹ A central question in this paper is whether this temperature window for etching can be predicted computationally.

The change in the integrated absorbance during each HF exposure can also be related to the thickness of the TiO_2 ALD film. From the results in Figure 7, an integrated absorbance (units of absorbance $\times \text{cm}^{-1}$) of 118 cm^{-1} is obtained from 400 to 960 cm^{-1} after 36 TiO_2 ALD cycles at 200 °C. Previous TiO_2 ALD studies have measured a TiO_2 ALD growth rate of 0.4 Å/cycle using TiCl_4 and H_2O as the reactants at 200 °C. Using this growth rate, the integrated absorbance of 118 cm^{-1} after 36 TiO_2 ALD cycles can be equated to a TiO_2 ALD film thickness of 14.4 Å. Using this correlation between integrated absorbance and TiO_2 film thickness, the TiO_2 film thickness removed for the HF exposure of 200 mTorr for 2 s at 300 °C is estimated to be 0.5 Å.

Figure 11 shows the Arrhenius plot of the temperature-dependent etch rates. This plot of the logarithm of the etch

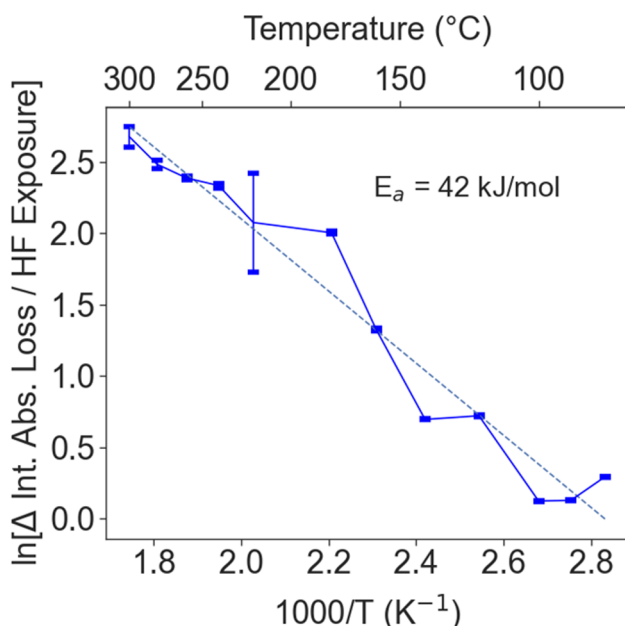


Figure 11. Arrhenius plot obtained from etch rates versus temperature presented in Figure 10. Slope of the plot yields an activation barrier of $E_a = 42 \text{ kJ/mol}$.

rate versus $1/T$ is approximately linear. The slope of the Arrhenius plot yields an activation energy of $E_a = 42 \text{ kJ/mol}$. This activation energy is presumably associated with the kinetics of the rate-limiting mechanistic step during HF etching of TiO_2 .

III.B.2. QMS Spectrometry. Quadrupole mass spectrometry was used to investigate the volatile etch species produced when HF interacts with TiO_2 at 300 °C. Figure 12a shows the mass spectrum from 46 to 110 amu that reveals the peaks for TiF_x^+ , TiF_2^+ , TiF^+ , and Ti^+ . The TiF_3^+ fragments have the highest intensity. The main fragment for TiF_3^+ is at $m/z = 105$ amu. These titanium fluoride species are assigned to the cracking fragments of TiF_4^+ . The small peaks found at 55 and 57 amu correspond to hydrocarbons that are often observed during heating of the filament for electron impact ionization.

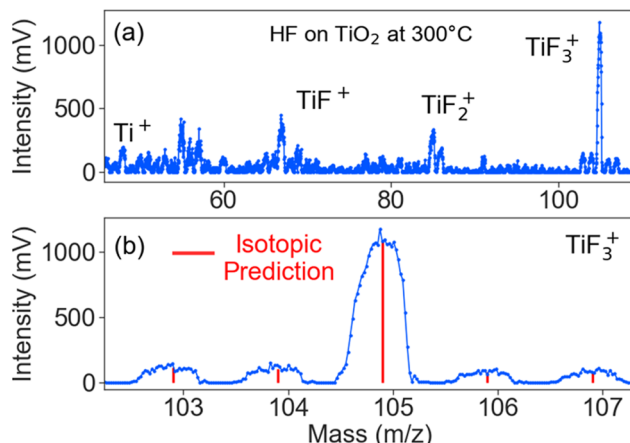


Figure 12. (a) TiF_x^+ mass species observed during HF exposure on TiO_2 powder at 300 °C. (b) Expansion of the mass range around the main TiF_3^+ fragment at $m/z = 105$ amu showing the measured signals and the predicted signals based on the Ti isotopes.

Figure 12b expands the mass spectrum around 105 amu. The TiF_3^+ fragment can be confirmed by the Ti isotopic ratios. Due to the isotopes of titanium, there should be expected peaks at 103, 104, 105, 106, and 107 amu with intensities of 10.8%, 9.9%, 100%, 7.5%, and 7.3%, respectively. These expectations accurately match the intensities of the peaks observed for the TiF_3^+ fragment. TiF_3^+ could be a fragment of TiF_4^+ . However, TiF_4^+ was not observed in the mass spectrum. TiF_4 is consistent with the CVE1 reaction where the expected product is $\text{TiF}_{4(g)}$. There also could be small contributions from the CVE3 reaction if the product was $\text{TiF}_{3(g)}$. TiF_3 is not likely as the parent because TiF_3 is a solid with a very high melting point of 1200 °C. In contrast, TiF_4 has a much lower melting point of 377 °C.

Figure 13 shows the intensity of the TiF_x^+ fragments during the HF exposure with a duration of 2 min. All TiF_x^+ fragments rise and fall with the HF exposure. The intensity of the TiF^+ peak has a higher background intensity resulting from small hydrocarbons desorbing from the filament at 86 amu. All the TiF_x^+ fragments are attributed to TiF_4 . The absence of the TiF_4 parent may result from its fragmentation during

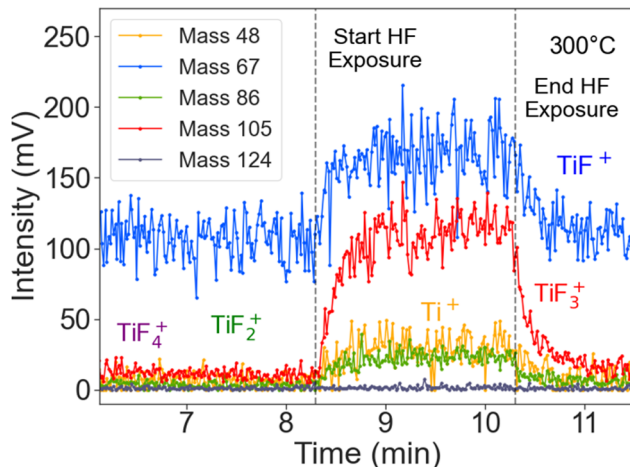


Figure 13. Mass spectrometry scans for TiF_4^+ , TiF_3^+ , TiF_2^+ , TiF^+ , and Ti^+ during an HF exposure lasting 2 min. All TiF_x^+ species rise and fall with the HF exposure.

ionization. Attempts to observe the TiF_4 parent were unsuccessful even when heating TiF_4 powder in a separate vacuum chamber equipped with a mass spectrometer.⁵⁰

Figure 14a shows the increase in the H_2O^+ intensity at 18 amu, and Figure 14b shows the increase in the HF^+ intensity at

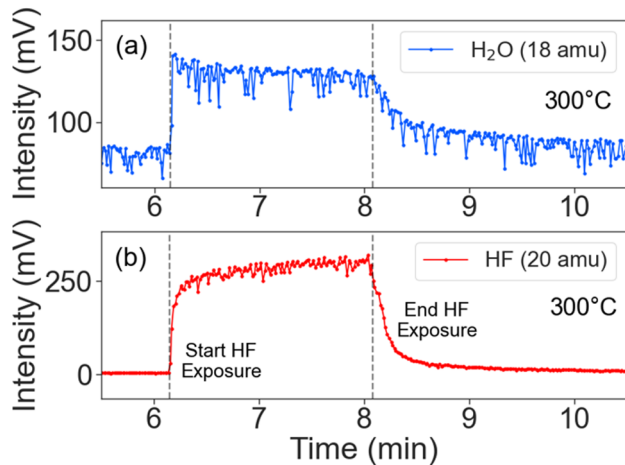


Figure 14. Mass spectrometry scans for (a) H_2O^+ and (b) HF^+ during an HF exposure lasting 2 min. The H_2O^+ intensity rises and falls with the HF exposure.

20 amu during the HF exposure with a duration of 2 min. The H_2O^+ signal rises and falls with the HF exposure. H_2O is an expected product of both the CVE1 and CVE3 reactions where $\text{TiF}_{4(g)}$ and $\text{TiF}_{3(g)}$ are the respective products. The mass signal for O_2 at 32 amu did not have an increase during the HF exposure. After the etching experiments, the mass of the powder was measured to investigate the mass decrease resulting from etching. The final mass was 31.26 mg compared with 40.58 mg before etching. The etching resulted in a 23% decrease in the mass of the TiO_2 nanopowder.

IV. DISCUSSION

The FEPs of postulated SL and CVE reactions for HF exposure on TiO_2 were calculated over wide temperature and pressure ranges of interest. Experimental results were also obtained for the etch onset, etch rate versus temperature and etch products. The onset temperature was the first temperature where the change in the integrated FTIR absorbance of the Ti–O vibrational band was found to be non-negligible. The FTIR measurements showed that the spontaneous etch of TiO_2 (a CVE-type reaction) was favorable from an onset temperature of 80–90 °C, which agrees with the theoretical prediction that the continuous etching of TiO_2 by reaction CVE1 dominates at temperatures greater than 360 K (87 °C). In this case, the predicted onset temperature is based on crossover of the computed thermodynamics of the candidate etching reactions. The correlation between the experimental and theoretical onset temperature counters the common assumption that onset temperatures are exclusively a reflection of reaction kinetics. Whether this is a general finding remains to be seen in the future.

The calculations show that the surface remains completely passivated with Ti–F species due to the self-limiting SL1 reaction at temperatures below the onset temperature. The FTIR difference spectra in Figure 8 also show a persistent Ti–F signal and the loss of Ti–O signal after each HF pulse on the

TiO_2 surface at 280 °C (553 K). At this temperature, the HF pulse is predicted to be in the “preferred etching” state where both SL1 and CVE1 reactions are favorable and compete with each other, but with CVE1 more thermochemically favorable. The favorability of CVE1 explains why spontaneous etching and loss of Ti–O signal is observed in Figure 8. The Ti–F signal at the surface is observed because the FTIR measurement takes place after the HF exposure. The F-covered TiO_2 surface from the SL1 reaction is preserved because Ti–F is a favorable surface intermediate at this temperature.

The mass spectrometry measurements identify TiF_4 and H_2O as the volatile etch products during HF exposure on TiO_2 . These volatile etch products are consistent with the reaction products of the CVE1 reaction pathway that is computed to be favorable, i.e., $\text{TiO}_2 + 4\text{HF} \rightarrow \text{TiF}_4 + 2\text{H}_2\text{O}$. There were no observed TiOF_2 products in agreement with a thermodynamically unfavorable CVE2 reaction. There was also no detection of an O_2 etch product in agreement with the thermodynamically unfavorable SL3 pathway.

This computational model generates thermodynamic information from a few DFT calculations on relatively small systems (i.e., bulk crystal, gas-phase molecules, and idealized surface slabs), which makes the model suitable for screening large numbers of candidate chemistries and designing new ALE processes. To look at the mechanism and kinetics underlying the process would require more time-consuming calculations. We expect that such calculations would show which individual steps in the CVE1 reaction are responsible for the measured activation energy ($E_a = 42 \text{ kJ/mol}$, Figure 11). This activation energy may be the barrier for diffusion of Ti and O atoms from subsurface layers to the fluorinated surface, prior to desorption as TiF_4 and H_2O respectively.

V. CONCLUSION

A combined computational and experimental approach has been presented to understand the competition between self-limiting and continuous etch reactions in an ALE process using HF exposures on TiO_2 as an example. In situ FTIR spectroscopy was used to study etch rates and surface species during the etching of TiO_2 with HF exposure. In situ mass spectrometry was also employed to identify the volatile etch products. The HF exposure was predicted to continuously etch TiO_2 in the temperature window 360–770 K (87–497 °C). There was excellent agreement between the onset temperature for the TiO_2 spontaneous etching of 87 °C calculated by the simulations and threshold for absorbance change at 80–90 °C measured by FTIR spectroscopy. The calculations also determined that an increase in the reactant pressure did not alter the etching onset temperature of the preferred etching pathway.

HF was predicted to passivate the TiO_2 surface with Ti–F species in a self-limiting reaction at temperatures up to 360 K (87 °C), and FTIR spectroscopy confirmed the presence of Ti–F surface species after HF exposures. The calculations predicted that TiO_2 was more favorably etched as TiF_4 rather than TiF_3 or TiOF_2 , and this was confirmed by the observation of cracking fragments of TiF_4 in mass spectrometry.

This study illustrates that the competition between self-limiting and continuous reactions can be predicted with straightforward DFT calculations and used to determine the temperature window for ALE processes. In addition, theory can predict the expected volatile etch products and surface species resulting from the self-limiting reactions. This

theoretical approach has also been experimentally validated using HF exposures on TiO₂. These theoretical predictions can therefore guide experiments so as to more efficiently develop viable ALE processes. This method of understanding the competition between self-limiting and continuous reactions should be useful for rapid high-throughput screening of precursors and various substrates to design new thermal ALE processes.

■ ASSOCIATED CONTENT

SI Supporting Information

The Supporting Information is available free of charge at <https://pubs.acs.org/doi/10.1021/acs.jpcc.1c08110>.

Convergence tests on unrelaxed surface models, free energy tables, entropy and free energy comparison, and free energy profiles on changes in product pressure ([PDF](#))

■ AUTHOR INFORMATION

Corresponding Author

Suresh Kondati Natarajan — Tyndall National Institute, University College Cork, Cork T12 RSCP, Ireland; Department of Electrical Engineering and Automation, Aalto University, Espoo 02150, Finland; [orcid.org/0000-0002-7018-5253](#); Email: suresh0807@gmail.com

Authors

Austin M. Cano — Department of Chemistry, University of Colorado, Boulder, Colorado 80309, United States
Jonathan L. Partridge — Department of Chemistry, University of Colorado, Boulder, Colorado 80309, United States
Steven M. George — Department of Chemistry, University of Colorado, Boulder, Colorado 80309, United States; [orcid.org/0000-0003-0253-9184](#)
Simon D. Elliott — Schrödinger Inc., New York, New York 10036-4041, United States; [orcid.org/0000-0001-5573-5694](#)

Complete contact information is available at:

<https://pubs.acs.org/10.1021/acs.jpcc.1c08110>

Notes

The authors declare no competing financial interest.

■ ACKNOWLEDGMENTS

The work at the University of Colorado was funded by Intel Corporation through a directed research grant from the Semiconductor Research Corporation. Additional support for the new mass spectrometry apparatus was provided by Lam Research. S.K.N. and S.D.E. thank the Irish Centre for High-End Computing (project code: tiche077c) and the Science Foundation Ireland funded computing cluster at Tyndall for the computer time.

■ REFERENCES

- (1) George, S. M. Atomic Layer Deposition: An Overview. *Chem. Rev.* **2010**, *110*, 111–131.
- (2) Puurunen, R. L. Surface chemistry of atomic layer deposition: A case study for the trimethylaluminum/water process. *J. Appl. Phys.* **2005**, *97*, 121301.
- (3) Elliott, S. D. Atomic-Scale Simulation of ALD Chemistry. *Semicond. Sci. Technol.* **2012**, *27*, 074008.

(4) Kim, H.; Lee, H. B. R.; Maeng, W. J. Applications of Atomic Layer Deposition to Nanofabrication and Emerging Nanodevices. *Thin Solid Films* **2009**, *517*, 2563–2580.

(5) Knez, M.; Nielsch, K.; Niinisto, L. Synthesis and Surface Engineering of Complex Nanostructures by Atomic Layer Deposition. *Adv. Mater.* **2007**, *19*, 3425–3438.

(6) George, S. M.; Lee, Y. Prospects for Thermal Atomic Layer Etching Using Sequential, Self-Limiting Fluorination and Ligand-Exchange Reactions. *ACS Nano* **2016**, *10*, 4889–4894.

(7) Kanarik, K. J.; Lill, T.; Hudson, E. A.; Sriraman, S.; Tan, S.; Marks, J.; Vahedi, V.; Gottscho, R. A. Overview of Atomic Layer Etching in the Semiconductor Industry. *J. Vac. Sci. Technol., A* **2015**, *33*, 020802.

(8) Song, S. K.; Saare, H.; Parsons, G. N. Integrated Isothermal Atomic Layer Deposition/Atomic Layer Etching Supercycles for Area-Selective Deposition of TiO₂. *Chem. Mater.* **2019**, *31*, 4793–4804.

(9) George, S. M. Mechanisms of Thermal Atomic Layer Etching. *Acc. Chem. Res.* **2020**, *53*, 1151–1160.

(10) Lee, Y.; George, S. M. Atomic Layer Etching of Al₂O₃ Using Sequential, Self-limiting Thermal Reactions with Sn(acac)₂ and Hydrogen Fluoride. *ACS Nano* **2015**, *9*, 2061–2070.

(11) Tan, S.; Yang, W.; Kanarik, K. J.; Lill, T.; Vahedi, V.; Marks, J.; Gottscho, R. A. Highly Selective Directional Atomic Layer Etching of Silicon. *ECS J. Solid State Sci. Technol.* **2015**, *4*, N5010–N5012.

(12) Fischer, A.; Routzahn, A.; George, S. M.; Lill, T. Thermal Atomic Layer Etching: A Review. *J. Vac. Sci. Technol., A* **2021**, *39*, 030801.

(13) Mullins, R.; Kondati Natarajan, S.; Elliott, S. D.; Nolan, M. Self-Limiting Temperature Window for Thermal Atomic Layer Etching of HfO₂ and ZrO₂ Based on the Atomic-Scale Mechanism. *Chem. Mater.* **2020**, *32*, 3414–3426.

(14) Filatova, E. A.; Hausmann, D.; Elliott, S. D. Investigating Routes Toward Atomic Layer Deposition of Silicon Carbide: Ab initio Screening of Potential Silicon and Carbon Precursors. *J. Vac. Sci. Technol., A* **2017**, *35*, 01B103.

(15) Lee, Y.; George, S. M. Thermal Atomic Layer Etching of HfO₂ Using HF for Fluorination and TiCl₄ for Ligand-Exchange. *J. Vac. Sci. Technol., A* **2018**, *36*, 061504.

(16) Lee, Y.; Huffman, C.; George, S. M. Selectivity in Thermal Atomic Layer Etching Using Sequential, Self-Limiting Fluorination and Ligand-Exchange Reactions. *Chem. Mater.* **2016**, *28*, 7657–7665.

(17) Lemaire, P. C.; Parsons, G. N. Thermal Selective Vapor Etching of TiO₂: Chemical Vapor Etching via WF₆ and Self-Limiting Atomic Layer Etching Using WF₆ and BCl₃. *Chem. Mater.* **2017**, *29*, 6653–6665.

(18) Xie, W.; Lemaire, P. C.; Parsons, G. N. Thermally Driven Self-Limiting Atomic Layer Etching of Metallic Tungsten Using WF₆ and O₂. *ACS Appl. Mater. Interfaces* **2018**, *10*, 9147–9154.

(19) Lemaire, P. C.; Parsons, G. N. Thermal Selective Vapor Etching of TiO₂: Chemical Vapor Etching via WF₆ and Self-Limiting Atomic Layer Etching Using WF₆ and BCl₃. *Chem. Mater.* **2017**, *29*, 6653–6665.

(20) Chase, M. W. *NIST-JANAF Thermochemical Tables*; 4th ed.; American Institute of Physics: 1998.

(21) Roine, A. HSC Chemistry for Windows—Chemical Reaction and Equilibrium Software with Extensive Thermochemical Database. *Outokumpu, HSC chemistry for Windows—Chemical ReOutokumpu Research Oy. Pori*, 1999.

(22) Kanarik, K. J.; Tan, S.; Yang, W.; Kim, T.; Lill, T.; Kabansky, A.; Hudson, E. A.; Ohba, T.; Nojiri, K.; Yu, J.; Wise, R.; Berry, I. L.; Pan, Y.; Marks, J.; Gottscho, R. A. Predicting Synergy in Atomic Layer Etching. *J. Vac. Sci. Technol., A* **2017**, *35*, 05C302.

(23) Kondati Natarajan, S.; Elliott, S. D. Modeling the Chemical Mechanism of the Thermal Atomic Layer Etch of Aluminum Oxide: A Density Functional Theory Study of Reactions during HF Exposure. *Chem. Mater.* **2018**, *30*, 5912–5922.

(24) Diebold, U. The Surface Science of Titanium Dioxide. *Surf. Sci. Rep.* **2003**, *48*, 53–229.

- (25) Fujishima, A.; Zhang, X. T.; Tryk, D. A. TiO₂ Photocatalysis and Related Surface Phenomena. *Surf. Sci. Rep.* **2008**, *63*, 515–582.
- (26) Wong, H. S. P.; Lee, H. Y.; Yu, S. M.; Chen, Y. S.; Wu, Y.; Chen, P. S.; Lee, B.; Chen, F. T.; Tsai, M. J. Metal-Oxide RRAM. *Proc. IEEE* **2012**, *100*, 1951–1970.
- (27) Niemelä, J.-P.; Marin, G.; Karppinen, M. Titanium Dioxide Thin Films by Atomic Layer Deposition: A Review. *Semicond. Sci. Technol.* **2017**, *32*, 093005.
- (28) Ritala, M.; Leskela, M.; Nykanen, E.; Soininen, P.; Niinisto, L. Growth of Titanium Dioxide Thin Films by Atomic Layer Epitaxy. *Thin Solid Films* **1993**, *225*, 288–295.
- (29) Lee, Y.; George, S. M. Thermal Atomic Layer Etching of Titanium Nitride Using Sequential, Self-limiting Reactions: Oxidation to TiO₂ and Fluorination to Volatile TiF₄. *Chem. Mater.* **2017**, *29*, 8202–8210.
- (30) Kresse, G.; Furthmüller, J. Efficient Iterative Schemes for Ab Initio Total-Energy Calculations Using a Plane-Wave Basis Set. *Phys. Rev. B: Condens. Matter Mater. Phys.* **1996**, *54*, 11169–11186.
- (31) Perdew, J. P.; Burke, K.; Ernzerhof, M. Generalized Gradient Approximation Made Simple. *Phys. Rev. Lett.* **1996**, *77*, 3865–3868.
- (32) Blochl, P. E. Projector Augmented-Wave Method. *Phys. Rev. B: Condens. Matter Mater. Phys.* **1994**, *50*, 17953–17979.
- (33) Kresse, G.; Joubert, D. From Ultrasoft Pseudopotentials to the Projector Augmented-Wave Method. *Phys. Rev. B: Condens. Matter Mater. Phys.* **1999**, *59*, 1758–1775.
- (34) Togo, A.; Tanaka, I. First Principles Phonon Calculations in Materials Science. *Scr. Mater.* **2015**, *108*, 1–5.
- (35) Kääriäinen, M. L.; Kääriäinen, T. O.; Cameron, D. C. Titanium Dioxide Thin Films, Their Structure and its Effect on Their Photoactivity and Photocatalytic Properties. *Thin Solid Films* **2009**, *517*, 6666–6670.
- (36) Balasubramani, S. G.; Chen, G. P.; Coriani, S.; Diedenhofen, M.; Frank, M. S.; Franzke, Y. J.; Furche, F.; Grotjahn, R.; Harding, M. E.; Hättig, C.; Hellweg, A.; Helmich-Paris, B.; Holzer, C.; Huniar, U.; Kaupp, M.; Marefat Khah, A.; Karbalaei Khani, S.; Müller, T.; Mack, F.; Nguyen, B. D.; Parker, S. M.; Perlt, E.; Rappoport, D.; Reiter, K.; Roy, S.; Rückert, M.; Schmitz, G.; Sierka, M.; Tapavicza, E.; Tew, D. P.; Van Wüllen, C.; Voora, V. K.; Weigend, F.; Wodynski, A.; Yu, J. M. TURBOMOLE: Modular Program Suite for Ab initio Quantum-Chemical and Condensed-Matter Simulations. *J. Chem. Phys.* **2020**, *152*, 184107.
- (37) Ferguson, J. D.; Weimer, A. W.; George, S. M. Atomic Layer Deposition of Ultrathin and Conformal Al₂O₃ films on BN Particles. *Thin Solid Films* **2000**, *371*, 95–104.
- (38) DuMont, J. W.; George, S. M. Pyrolysis of Alucone Molecular Layer Deposition Films Studied Using in Situ Transmission Fourier Transform Infrared Spectroscopy. *J. Phys. Chem. C* **2015**, *119*, 14603–14612.
- (39) Ferguson, J. D.; Yoder, A. R.; Weimer, A. W.; George, S. M. TiO₂ Atomic Layer Deposition on ZrO₂ Particles Using Alternating Exposures of TiCl₄ and H₂O. *Appl. Surf. Sci.* **2004**, *226*, 393–404.
- (40) Saric, I.; Peter, R.; Piltaver, I. K.; Badovinac, I. J.; Salamon, K.; Petracic, M. Residual Chlorine in TiO₂ Films Grown at Low Temperatures by Plasma Enhanced Atomic Layer Deposition. *Thin Solid Films* **2017**, *628*, 142–147.
- (41) Lii-Rosales, A.; Cavanagh, A. S.; Fischer, A.; Lill, T.; George, S. M. Spontaneous Etching of Metal Fluorides Using Ligand-Exchange Reactions: Landscape Revealed by Mass Spectrometry. *Chem. Mater.* **2021**, *33*, 7719–7730.
- (42) Peng, G. W.; Chen, S. K.; Liu, H. S. Infrared-Absorption Spectra and Their Correlation with the Ti-O Bond-Length Variations for TiO₂ (Rutile), Na-Titanates and Na-Titanosilicate (Natisite, Na₂TiOSiO₄). *Appl. Spectrosc.* **1995**, *49*, 1646–1651.
- (43) Madhusudan Reddy, K.; Gopal Reddy, C.V.; Manorama, S.V. Preparation, Characterization, and Spectral Studies on Nanocrystalline Anatase TiO₂. *J. Solid State Chem.* **2001**, *158*, 180–186.
- (44) DuMont, J. W.; Marquardt, A. E.; Cano, A. M.; George, S. M. Thermal Atomic Layer Etching of SiO₂ by a “Conversion-Etch” Mechanism Using Sequential Reactions of Trimethylaluminum and Hydrogen Fluoride. *ACS Appl. Mater. Interfaces* **2017**, *9*, 10296–10307.
- (45) Queeney, K. T.; Weldon, M. K.; Chang, J. P.; Chabal, Y. J.; Gurevich, A. B.; Sapjeta, J.; Opila, R. L. Infrared Spectroscopic Analysis of the Si/SiO₂ Interface Structure of Thermally Oxidized Silicon. *J. Appl. Phys.* **2000**, *87*, 1322–1330.
- (46) Liu, J. C. M-x-O-y-Si-z Bonding Models for Silica-Supported Ziegler-Natta Catalysts. *Appl. Organomet. Chem.* **1999**, *13*, 295–302.
- (47) Ricchiardi, G.; Damin, A.; Bordiga, S.; Lamberti, C.; Spano, G.; Rivetti, F.; Zecchina, A. Vibrational Structure of Titanium Silicate Catalysts. A Spectroscopic and Theoretical Study. *J. Am. Chem. Soc.* **2001**, *123*, 11409–11419.
- (48) Beattie, I. R.; Jones, P. J. The Infrared Spectrum of the Nu-3 Band of TiF₄ - Comment. *J. Chem. Phys.* **1989**, *90*, 5209–5210.
- (49) Beattie, I. R.; Jones, P. J.; Young, H. A. Do Any AB_n Molecules Have Anomalous Shapes? Nu-3 of TiF₄ and TiF₃ and Their Relevance to the Shape of TiF₂. *Angew. Chem., Int. Ed. Engl.* **1989**, *28*, 313–315.
- (50) Clancey, J. W.; Cavanagh, A. S.; Smith, J. E. T.; Sharma, S.; George, S. M. Volatile Etch Species Produced during Thermal Al₂O₃ Atomic Layer Etching. *J. Phys. Chem. C* **2020**, *124*, 287–299.

■ NOTE ADDED AFTER ASAP PUBLICATION

This paper was published ASAP on November 12, 2021, with errors in the text. The corrected version was reposted on November 15, 2021.